



Electrical properties of Nb/Al-doped CuO-based ceramics for NTC thermistors

Xianchi Wang, Zhicheng Li, Weiqin Yan, Pinji Wang, Hong Zhang*

School of Materials Science and Engineering, Central South University, Changsha 410083, China

Received 11 November 2019; Received in revised form 10 January 2020; Accepted 11 February 2020

Abstract

Nb/Al-modified CuO ceramics ($y\text{Nb}/0.02\text{Al-CuO}$, $0 \leq y \leq 0.07$, denoted as NACO) were synthesized using sol-gel method for applications in negative temperature coefficient (NTC) thermistors. The phase structure, microstructure and electrical properties of the ceramics were investigated. XRD investigation reveals that the NACO ceramics has the main phase with monoclinic crystalline structure. The analysis of X-ray photoelectron spectroscopy proved the existence of $\text{Cu}^{2+}/\text{Cu}^+$ and $\text{Nb}^{5+}/\text{Nb}^{4+}$ ions. Temperature dependence of the resistivity indicated that the NACO ceramics present typical NTC characteristic. The NTC materials' constant, B value, can be adjusted from 2430 K to 3805 K by changing the Nb-concentration in the Al-doped CuO ceramics. Among four applied calibration equations the Hoge-3 equation is the most effective one for the resistance-temperature calibration of the prepared NTC thermistors. The complex impedance analysis was performed and revealed that both grain effect and grain boundary effect similarly contribute to the electrical conductive behaviour and NTC feature of the NACO ceramics. The band conduction and polaron hopping conduction are proposed as the conduction mechanisms in the NACO thermistors.

Keywords: CuO ceramics, electrical property, impedance spectroscopy, thermistors, conduction mechanism

I. Introduction

In the last decades the thermistors with negative temperature coefficient (NTC) of resistivity have been recognized as the effective electronic elements in thermal sensors. This is because NTC thermistors generally own a unique characteristic that the resistivity decreases exponentially with the increase of temperature. The commercial NTC thermistors are always made of polycrystalline semiconductor ceramics and have AB_2O_4 -type spinel structure [1–3]. The conduction mechanism of NTC thermistor with spinel structure is usually considered to be small polaron hopping model, in which charge carriers hop between the octahedral B-sites, at which valence-variable cations are located, e.g. the polarons hop between Mn^{3+} and Mn^{4+} ions in spinel magnetite. The electrical properties of spinel thermistors are closely related to ionic distribution and even the fabrication process [1–6]. Sintering conditions such as sintering temperature and atmosphere have a close influence on the oxidation state of B-site cations in spinel and

then a slight change of sintering conditions might affect the room-temperature resistivity (ρ_{25}) and temperature sensitivity [7]. Moreover, structural relaxation leads to the performance degradation always occurring in those thermistors. In order to prepare the NTC thermistors with better properties, numerous studies have been performed, e.g. cation doping and element substitution [8], perovskite compounds [9], spinel ferrite [10], composite thermistors composed of perovskite and spinel compounds [11], etc.

Recently, some studies focused on the preparation of single-component oxide NTC ceramics, in which the doping with transition metal elements was usually achieved. Compared with the multi-component NTC ceramics, single-component oxide NTC ceramics have the advantages of adjustable temperature sensitivity (in NTC material also called B value) and room temperature resistivity (ρ_{25}). To a specific NTC thermistor system, it should be of practical application value to achieve both adjustable ρ_{25} and appropriate B values by element doping. Ceramics based on single oxides such as SnO_2 , NiO , CuO and vanadium oxides were studied due to their excellent NTC characteristics, and both ρ_{25}

*Corresponding authors: tel: +86 731 88876692, e-mail: hzhang@csu.edu.cn

and B value can be effectively adjusted by oxide doping and element substitution [12–18]. Copper oxide (CuO), a semiconducting material with a band gap of about 1.4 eV, is one of the widely used materials because of its unique electrical conductivity, optical/catalytic properties, chemical stability and low cost [19]. Numerous application interests such as solar cells, lithium ion batteries, super capacitors, gas sensors, dielectric feature and magnetic storage materials, etc. have arisen [19–24]. Recent studies have shown that the CuO based ceramics have the potential applications in NTC thermistors. For example, in Ti/Y-modified CuO-based NTC thermistors, the B values could be adjusted from 1112 to 3700 K, and the ρ_{25} ranging from 80 to $2.75 \times 10^6 \Omega \cdot \text{cm}$ were achieved [25].

In this work, Al-doped CuO (ACO) and Nb/Al-codoped CuO-based (NACO) ceramics were prepared and investigated. The prepared CuO-based ceramics show the characteristics of adjustable ρ_{25} and B values. The electrical properties of the prepared ceramics were studied in detail. On the other hand, NTC thermistor generally shows a certain resistance at a certain temperature. To express the relationship between the resistance and temperature in a temperature measurement system, the suitable calibration equation is used to convert the measured resistance values of thermistor to the corresponding temperature values [26]. In this report, four calibration equations are used to evaluate the fitting consistency of resistance-temperature data of prepared NTC thermistors.

II. Experimental procedure

2.1. Ceramic preparation

Al-doped CuO ($x\text{Al-CuO}$, denoted as ACO, $x = 0, 0.005, 0.01, 0.015, 0.02, 0.025, 0.03$ and 0.04) and Nb-modified 0.02Al-CuO ($y\text{Nb}/0.02\text{Al-CuO}$, denoted as NACO, $y = 0, 0.01, 0.02, 0.03, 0.04, 0.05$ and 0.07) powders were synthesized by sol-gel method. As the starting materials, appropriate quantities of copper hydroxide ($\text{Cu}(\text{OH})_2$, >94.0%, Aladdin Chemical, China), aluminium nitrate ($\text{Al}(\text{NO}_3)_3 \cdot 9\text{H}_2\text{O}$, >99.0%, Xilong Chemical, China) and niobium oxalate ($\text{C}_{10}\text{H}_5\text{NbO}_{20}$, concentration of niobium is 16.69 wt.%, Ningxia Orient Tantalum Industry Co., Ltd, China) were weighed according to the designed composition of the $y\text{Nb}/0.02\text{Al-CuO}$ in each batch. Copper hydroxide was dissolved in the diluted nitric acid solution, while aluminium nitrate and niobium oxalate were dissolved in the hot deionized water. Two solutions were mixed together and then the prepared solution mixture was magnetically stirred, heated and finally dried to acquire precursor. The precursors were calcined at 830°C for 5 h in air and then the calcined mixture was crushed and ground to obtain fine powders.

The related CuO-based ceramics were prepared by traditional ceramic process. The calcined powders were granulated with PVA solution, and were pressed into

disks with 12 mm in diameter and about 3 mm in thick. The green pellets were sintered at $980\text{--}1000^\circ\text{C}$ for 30 min in air. In addition, the sintered ceramics were polished into discs with thickness of approximately 2 mm. In order to measure the electrical properties, silver paste was coated on both surfaces and heated at 600°C for about 5 min to make the ohmic electrodes.

2.2. Structure characterization

The crystalline phases of the sintered ceramic samples were analysed by X-ray diffraction (XRD) on Rigaku D/max 2500, Japan diffractometer using $\text{Cu K}\alpha$ radiation ($\lambda = 0.154056 \text{ nm}$) at a scanning rate of $8^\circ/\text{min}$. A scanning electron microscope (SEM, FEI Quanta200) was applied to investigate the ceramic microstructure on the fresh fractured surfaces. X-ray photoelectron spectroscopy (XPS, K-alpha 1063, UK) was adopted to analyse the valence states of Cu- and Nb-ions of the sintered ceramics.

2.3. Properties test

The resistance-temperature (R - T) data of the prepared samples were obtained by a resistance-temperature measurement system (ZWX-C, China) in the temperature range $25\text{--}250^\circ\text{C}$. The resistivity (ρ) was calculated by Eq. 1:

$$\rho = R \frac{\pi \cdot r^2}{h} \quad (1)$$

where, R is the measured resistances, r and h are radius and thickness of the sample, respectively. The MATLAB software was used to analyse the resistance-temperature data of the samples. Four different calibration equations (the Basic equation, Steinhart-Hart equation, Hoge-2 equation and Hoge-3 equation) were used to fit the experimental resistance-temperature data of $0.03\text{Nb}/0.02\text{Al-CuO}$ and $0.05\text{Nb}/0.02\text{Al-CuO}$ thermistors in temperature range from 25 to 150°C .

The alternating current (AC) impedance measurements were carried out by an electrochemistry test system (Gamry Reference 600, USA) with the test frequency range from 1 Hz to 1 MHz, in the temperature range $25\text{--}200^\circ\text{C}$.

III. Results and discussion

3.1. Phase and microstructure

Figure 1 shows the XRD patterns of an undoped CuO ceramics sintered at 980°C for 30 min and the NACO samples ($y = 0, 0.02, 0.04$) sintered at 1000°C for 30 min. Through refinement analysis of the diffraction patterns with Jade 6.0 program, the undoped CuO, 0.02Al-CuO and $0.02\text{Nb}/0.02\text{Al-CuO}$ samples exhibit a single monoclinic CuO phase (PDF No. 89-5897) with space group of $C2/c$. The $0.04\text{Nb}/0.02\text{Al-CuO}$ ceramics has a slight extra diffraction peak that can be identified to be from Nb_2O_5 . The lattice parameters of the NACO

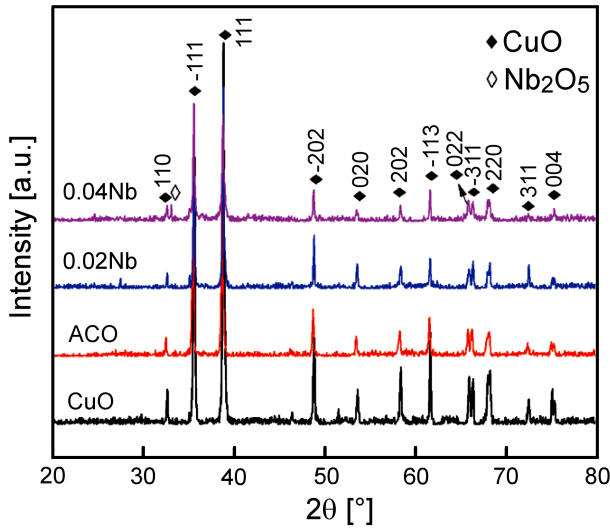


Figure 1. XRD patterns of sintered undoped CuO (CuO), 0.02Al-CuO (ACO), 0.02Nb/0.02Al-CuO (0.02Nb) and 0.04Nb/0.02Al-CuO (0.04Nb) ceramics

ceramics were obtained by the refinement of the XRD patterns and shown in Table 1. The lattice parameters of the 0.02Al-CuO ceramics have higher values than that of the undoped CuO. This might be the result of the occurrence of oxygen vacancies in the undoped CuO during the traditional ceramics sintering process [25]. The lattice parameters of the Nb/Al-doped CuO also have slightly higher values than those of the undoped CuO. The radii of Al³⁺ (0.053 nm) and Nb⁵⁺ ions (0.064 nm) are smaller than that of Cu²⁺ ions (0.073 nm), thus the substitution of Al- and Nb-ions should reduce slightly lattice parameters. However, the substitution of Al- and Nb-ions into the CuO lattice might attract oxygen ions and reduce the amount of oxygen vacancies, resulting in the slight increasing of lattice parameters in Nb/Al-doped CuO. A small extra diffraction peak could be detected as an impurity in Nb₂O₅ for the NACO with y = 0.04, indicating the limited solid solution of Nb₂O₅ in CuO. Meanwhile, the formation of oxygen vacancies and substitution of cations with different size from that

Table 1. The lattice parameters of the sintered ceramics

Sample	a [nm]	b [nm]	c [nm]	β [°]
undoped CuO	0.4681	0.3413	0.5112	99.52
0.02Al-CuO	0.4692	0.3427	0.5133	99.50
0.02Nb/0.02Al-CuO	0.4682	0.3419	0.5125	99.51
0.04Nb/0.02Al-CuO	0.4683	0.3429	0.5126	99.50

of Cu-ion lead to slight lattice distortion and different interaxial angle of β as shown in Table 1.

In order to investigate the possible valences of Cu- and Nb-cations, XPS spectra of Cu 2p and Nb 3d for 0.04Nb/0.02Al-CuO ceramics were analysed as shown in Fig. 2. A typical Cu 2p XPS spectrum is shown in Fig. 2a. The peak with binding energy of 933.6 eV accompanied by the satellite peaks at 941.1 and 943.7 eV corresponds to Cu 2p_{3/2} for Cu²⁺ ions, and the binding energy of 953.6 eV with the satellite peak located at 962.4 eV corresponds to Cu 2p_{1/2} for Cu²⁺ ions. The smaller peak at 932.9 eV should correspond to Cu 2p_{3/2} for Cu⁺ ions. This indicates that Cu²⁺ and Cu⁺ ions co-exist in 0.04Nb/0.02Al-CuO ceramics [27]. The high resolution XPS spectrum of Nb 3d is shown in Fig. 2b. According to the literature data [28] it is clear that the peak with binding energy of 206.5 eV corresponds to Nb⁴⁺ ions and the peak with binding energy of 209.4 eV should correspond to Nb⁵⁺ ions. This indicates the existence of Nb⁵⁺ and Nb⁴⁺ ions in the prepared ceramics.

SEM observations of the sintered yNb/0.02Al-CuO (y = 0.02 and y = 0.04) ceramics were performed and the typical images are illustrated in Fig. 3. The microstructures confirm that the NACO ceramics have good sintering characteristics even at low temperatures (980–1000 °C). The 0.02Nb ceramics (Fig. 3a) has similar microstructural characteristic to that of the 0.04Nb ceramics (Fig. 3b). Some small pores located between grains can also be seen. The density of the undoped CuO ceramics is 6.52 g·cm⁻³. According to the Archimedes principle of water displacement, compared with the density of the undoped CuO ceramics, the relative densities of the sintered yNb/0.02Al-CuO (y = 0, 0.01, 0.02, 0.03, 0.04, 0.05 and 0.07) ceramics were calculated to

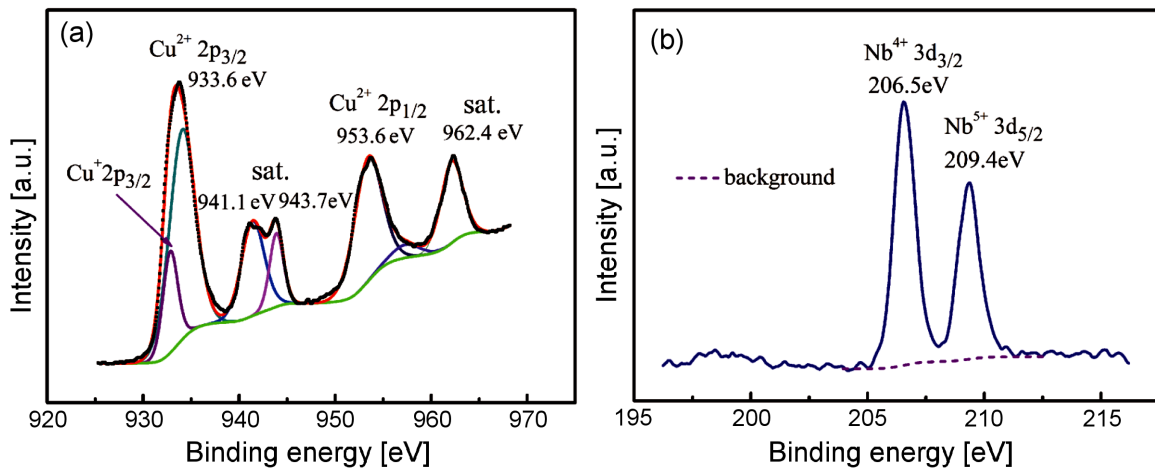


Figure 2. XPS spectra of 0.04Nb/0.02Al-CuO ceramics: a) Cu 2p and b) Nb 3d

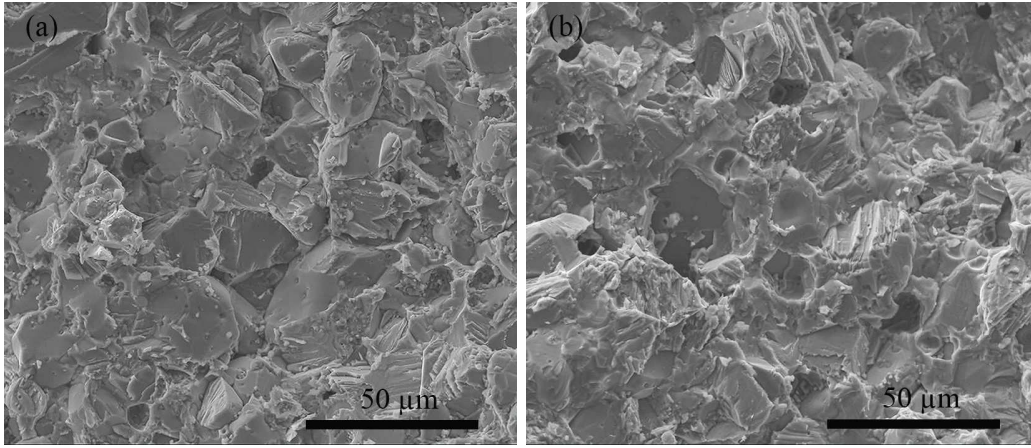


Figure 3. SEM micrographs of yNb/0.02Al-CuO ceramics for y: a) 0.02 and b) 0.04

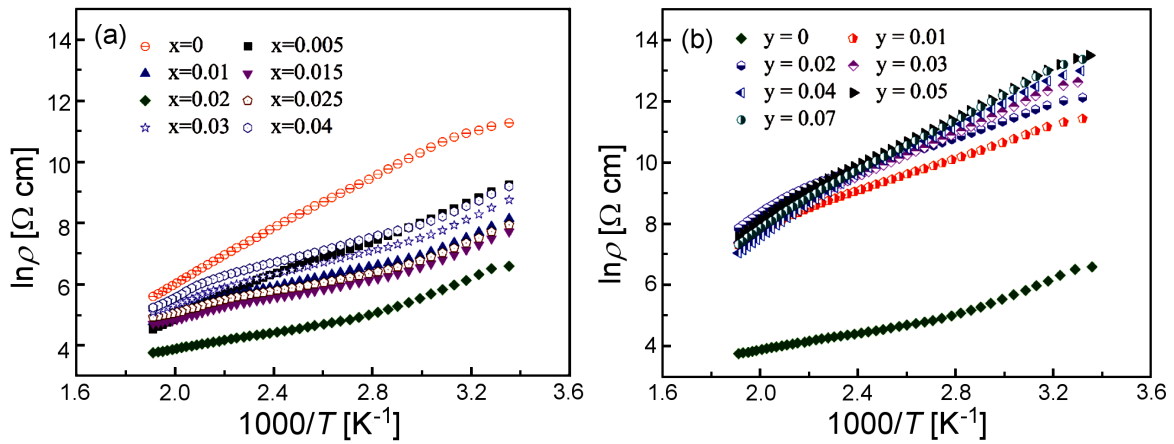


Figure 4. Temperature dependence of resistivity of CuO-based ceramics: a) xAl-CuO ($x = 0, 0.005, 0.01, 0.015, 0.02, 0.025, 0.03, 0.04$) and b) yNb/0.02Al-CuO ceramics ($y = 0, 0.01, 0.02, 0.03, 0.04, 0.05, 0.07$)

be 86.6, 91.2, 89.9, 90.7, 88.6, 89.4 and 89.6% TD, respectively.

3.2. Electrical properties

Figure 4a shows the concentration dependence of the resistivity ρ of the Al-doped CuO ceramics at different temperatures. It can be seen that the ACO ceramics shows a NTC characteristic. Two key factors of NTC thermistor, resistivity (ρ_T) and thermal sensitivity (B), are calculated by using the following equations:

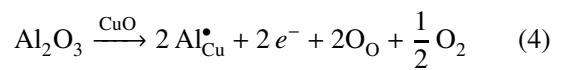
$$\rho_T = A \cdot \exp \frac{E_a}{k \cdot T} \quad (2)$$

$$B = \frac{\ln \rho_1 \cdot \ln \rho_2}{\frac{1}{T_1} - \frac{1}{T_2}} \quad (3)$$

where, ρ_T is resistivity at temperature T , k is the Boltzmann constant, A is a constant related to the material characteristic, E_a is activation energy of conduction, $B = E_a/k$ is the factor of thermal sensitivity. For convenience, T_1 and T_2 are often selected as 25 °C and 85 °C, respectively, and B value can be written as $B_{25/85}$.

Among all the xAl-CuO samples, the 0.02Al-CuO ceramics has the lowest resistivity and it was selected for further experiments and Nb-ion substitution to adjust

thermal sensitivity (B value). All the xAl-CuO ceramics show lower ρ_{25} value than the undoped CuO ceramics. These should be closely related to the donor doping of Al^{3+} ions. The corresponding defect chemistry reaction can be described by Eq. 4:



Al^{3+} ion acts as a donor in CuO crystal, in which the weakly bound electrons can be thermally activated to jump to the conduction band and provide electronic conduction. Element doping can effectively regulate the conductivity of a semiconductor material and there is an optimized dopant content for a certain material [12–18]. As shown in Fig. 4a, in the xAl-CuO the optimal donor concentration might be $x = 0.02$. The conductivity increases with the increase of Al^{3+} ion concentration when x is less than 0.02 due to the rise of charge carriers (electrons) concentration. The conductivity (σ) is proportional to the concentration of charge carriers (n), i.e. $\sigma = n \cdot e \cdot \mu$, where e is the electron charge and μ is the electron mobility. However, when x is higher than 0.02, the accumulation of charge carriers might take place and the conductivity decreases.

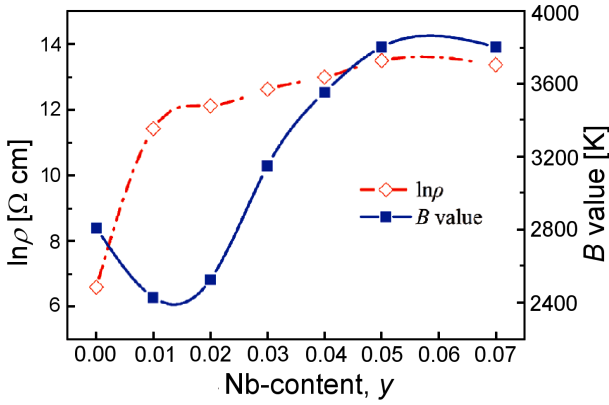
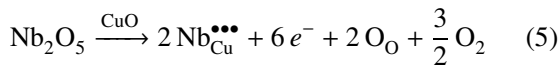


Figure 5. ρ_{25} and $B_{25/85}$ values as a function of Nb-concentration for NACO ceramics

Figure 4b shows the relationship between $\ln \rho$ and $1/T$ for the $y\text{Nb}/0.02\text{Al-CuO}$ ceramics with different Nb concentrations. Figure 5 shows the Nb-concentration dependence of ρ_{25} and $B_{25/85}$ of the NACO ceramics. It can be seen that all the $y\text{Nb}/0.02\text{Al-CuO}$ ceramics exhibit a typical NTC behaviour. The ρ_{25} of the Nb/Al-codoped CuO ceramics increases with the increase of concentration of Nb ions. The ρ_{25} are 7.25×10^2 , 9.16×10^4 , 1.88×10^5 , 3.03×10^5 , 4.39×10^5 , 7.26×10^5 and $6.37 \times 10^5 \Omega\cdot\text{cm}$ when the Nb-concentrations are $y = 0, 0.01, 0.02, 0.03, 0.04, 0.05$ and 0.07 , respectively. The $B_{25/85}$ values of the Nb/Al-doped CuO at first decrease and then increase, with the increase of concentration of Nb ions. The related $B_{25/85}$ values are 2803, 2430, 2526, 3157, 3552, 3805 and 3803 K for $y = 0, 0.01, 0.02, 0.03, 0.04, 0.05$ and 0.07 , respectively. It shows that the Nb/Al-doped CuO materials are suitable candidates for commercial thermistors, because the $B_{25/85}$ of commercial NTC thermistors is usually in the range of 2000–6000 K [29].

Similar to Eq. 4, the substitution of Nb^{5+} ions into CuO lattice may also produce weakly bound electrons as shown in Eq. 5:



For the prepared NACO ($y\text{Nb}/0.02\text{Al-CuO}$) ceramics which are Nb-modified 0.02Al-CuO samples, both Al^{3+} and Nb^{5+} ions co-substituted into CuO lattice would produce excessive electrons and cause the electron accumulation in the lattice, resulting in the rapid rise of conductivity. On the other hand, since Nb and Cu ions have different ionic radii, the substitution of Nb ions might result in lattice distortion that increased the local lattice barrier, resulting in the rise of resistivity. Also, higher amount of Nb_2O_5 leads to the formation of impurities and could also result in the rise of ρ_{25} . Both the lattice distortion and impurity also increased the activation energies of conduction, so the $B_{25/85}$ values increased with the introduction of Nb-ions in the Al-doped CuO ceramics.

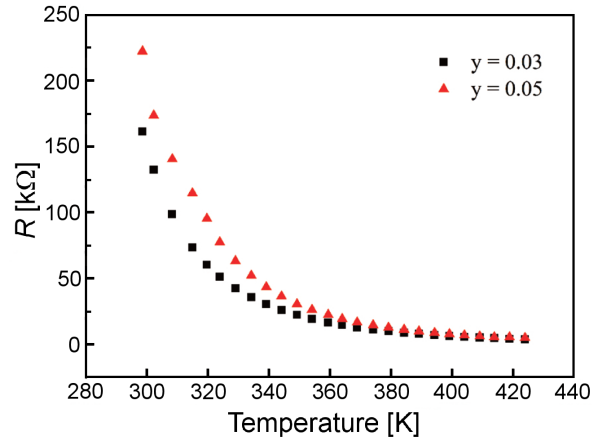


Figure 6. $R-T$ measurement data of $y\text{Nb}/0.02\text{Al-CuO}$ thermistors ($y = 0.03$ and $y = 0.05$)

Calibration equation directly affects the accuracy of thermistor for temperature measurement [26,30]. For the prepared NACO thermistor, it is necessary to select different calibration equations to fit its resistance-temperature data and find the best one. The $R-T$ data of the 0.03Nb/0.02Al-CuO and 0.05Nb/0.02Al-CuO thermistors measured in the range of 25–150 °C are shown in Fig. 6. Four calibration equations, the Basic, Steinhart-Hart, Hoge-2 and Hoge-3 equations, were selected to fit the resistance-temperature relationship of the 0.03Nb/0.02Al-CuO and 0.05Nb/0.02Al-CuO NTC thermistors. The Hoge-3 equation had the best calibration results among these four calibration equations for the NACO thermistors (for specific analysis please refer to *Supplementary material*).

3.3. AC impedance and electric modulus analysis

Analysis of AC impedance spectroscopy is one of the powerful methods to probe into electrical characters of ceramics. Figure 7 shows the Nyquist plots of the NACO ceramics with various Nb contents, measured at 25 °C and in frequencies ranging from 1 Hz to 1 MHz.

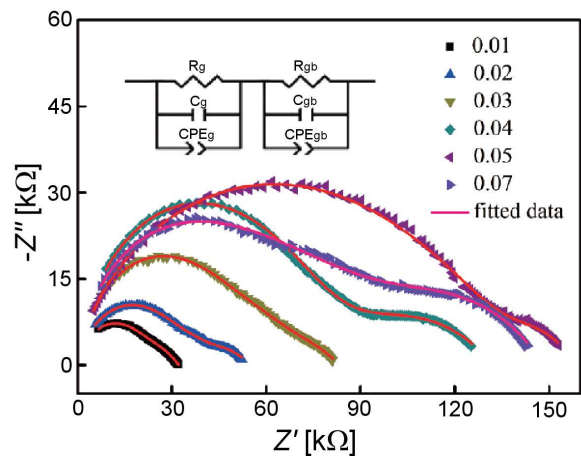


Figure 7. Complex impedance spectra of $y\text{Nb}/0.02\text{Al-CuO}$ ceramics ($y = 0.01, 0.02, 0.03, 0.04, 0.05$ and 0.07) measured at 25 °C (inset - equivalent circuit used for data fitting)

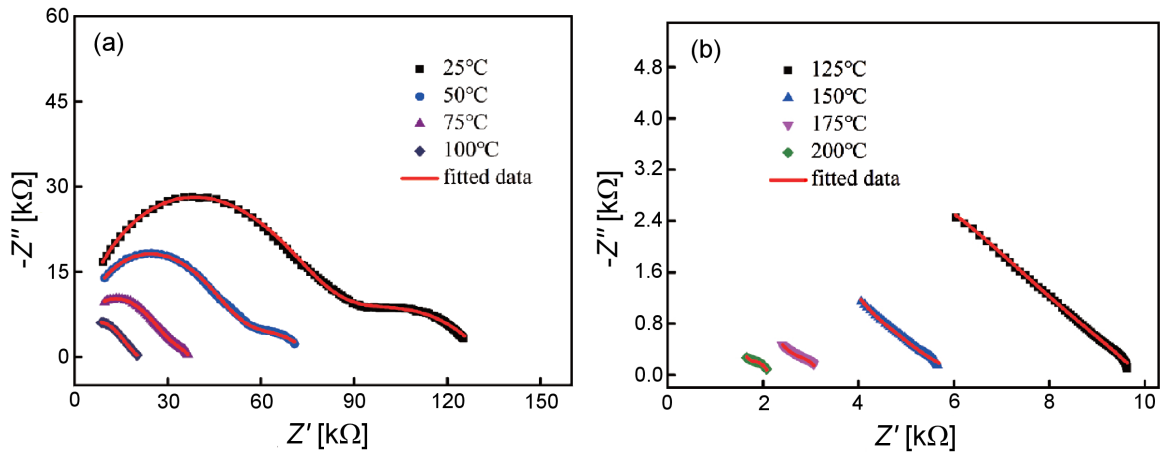


Figure 8. Complex impedance spectra of 0.04Nb/0.02Al-CuO ceramics measured at: a) 25, 50, 75 and 100 °C, and b) 125, 150, 175 and 200 °C

An equivalent circuit composed of two parallel R - C - CPE parts (inset in Fig. 7, where R is resistance, C is capacitance and CPE is constant phase element) was used to fit impedance spectra. In the present case, two arcs can be observed directly. The fitted curves are consistent with the experimental data. According to the fitted results as shown in Table S2 in the *Supplementary material*, one can see that the NTC effects of NACO samples come from both grain and grain-boundary. The resistance of the grain, R_g is always larger than the one from the grain-boundary effect R_{gb} in each y Nb/0.02Al-CuO ceramics. The total impedance ($R_g + R_{gb}$) increased with the increase of Nb concentration. Two types of relaxation time for two different relaxation processes can be calculated by the formula $\tau = R \cdot C$, where R is the resistance and C is the capacitance for grain or grain boundary response [31].

Figure 8 shows the typical Cole-Cole plots of the 0.04Nb/0.02Al-CuO ceramics at various temperatures. The impedance spectra measured at 25, 50, 75 and 100 °C consist obviously of two arcs representing the grain effect and grain-boundary effect, respectively. However, each impedance spectrum measured at tem-

peratures higher than 125 °C just show one arc. This should be attributed to the material characteristic and the frequency limit of the measurement system. The fitted results are shown in Table S3 in the *Supplementary material*. It is found that the total resistance ($R_g + R_{gb}$) decreases with the increase of temperature, which is the characteristic of typical NTC behaviour. The grain resistance (R_g) is higher than the grain-boundary one (R_{gb}) at each temperature.

Figure 9a shows the frequency dependence of imaginary part of impedance (Z'') of the 0.04Nb/0.02Al-CuO ceramics at various temperatures. It is obvious that the detectable relaxation peaks changed with the increase of temperature. Each plot shows two relaxation peaks when the measured temperature is below 50 °C, indicating that the electrical responses resulted from two parts which are grain-boundary effect in low frequency region and grain effect in the high frequency region. In the range 50–100 °C, each plot has one peak. When temperatures are higher than 100 °C, no relaxation peak can be observed; the possible relaxation peaks might be located at higher frequency region considering the limited measurement frequency.

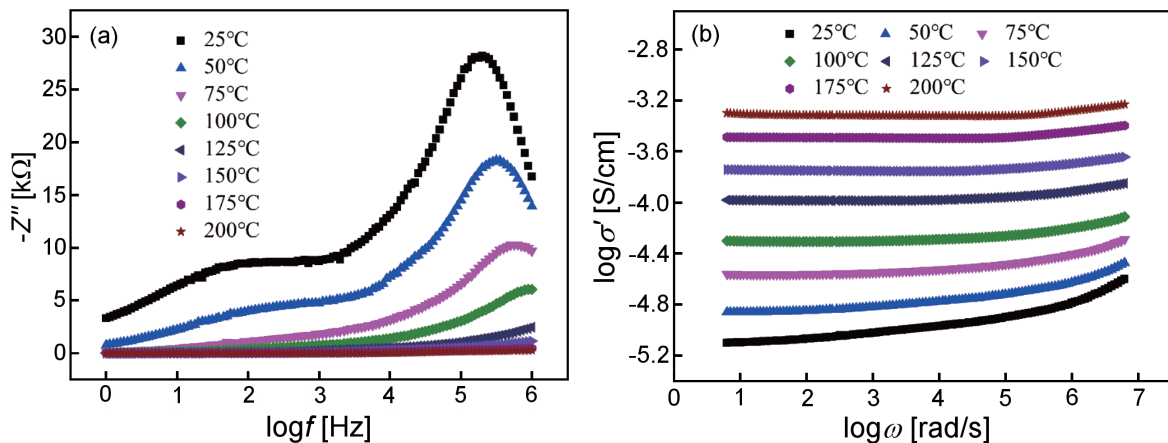


Figure 9. Temperature dependence of electrical properties of 0.04Nb/0.02Al-CuO ceramics: a) frequency dependence of the imaginary part of impedance (Z'') at various temperatures and b) double-logarithmic plots ($\log \sigma'(\omega)$ - $\log \omega$) at various temperatures

Figure 9b shows the double-logarithmic plot ($\log \sigma'(\omega)$ versus $\log \omega$) of the 0.04Nb/0.02Al-CuO ceramics at various temperatures. The results show that at each temperature, the AC conductance has a frequency-independent region and a frequency-dependent region. Compared with lower temperature, the frequency dependence of AC conductivity at higher temperatures is smaller. $\sigma'(\omega)$ can be described by the Jonscher power law, $\sigma'(\omega) = \sigma'(0) + \sigma_0(\omega)^S$; where ω is the angular frequency, $\sigma'(0)$ is the DC conductivity, σ_0 is the temperature dependent constant and S is the power exponent depending on temperature and material. The values of $\log \sigma'(\omega)$ were almost invariable in the low frequency region at each tested temperature. DC conductivity $\sigma'(0)$ increases with the increase of temperature, indicating that the long-range mobility of charge carriers becomes easier [32]. S is the slope of the $\log \sigma'(\omega)$ versus $\log \omega$ plot at frequency-dependent region, and the S values are 0.396, 0.403, 0.387, 0.402, 0.385, 0.449, 0.457 and 0.572 at temperatures of 25, 50, 75, 100, 125, 150, 175 and 200 °C, respectively. The S values are less than 1 at measured temperatures, confirming the presence of polaron hopping conduction mechanism in NACO ceramics. In the process of polaron jump conduction, there should be valence-variable ions with different valence states in the NACO ceramic lattice. It has been proved by X-ray photoelectron spectroscopy analysis that the $\text{Cu}^+/\text{Cu}^{2+}$ ion pairs and $\text{Nb}^{4+}/\text{Nb}^{5+}$ ion pairs coexist in the prepared CuO-based ceramics. Therefore, the contribution to the hopping conduction might mainly come from the Cu-ions such as $\text{Cu}^{2+} + \text{Cu}^+ \rightleftharpoons \text{Cu}^+ + \text{Cu}^{2+}$, and also from the Nb-ions such as $\text{Nb}^{5+} + \text{Nb}^{4+} \rightleftharpoons \text{Nb}^{4+} + \text{Nb}^{5+}$.

Further, Gerhardt [33] reported that the frequency dependence of the normalized imaginary impedance (Z''/Z''_{max}) and electrical modulus (M''/M''_{max}) can be used to distinguish localized conduction (i.e. short-range conduction) from the long-range conduction. Figure 10 shows the plots of $Z''/Z''_{max}-\log f$ and $M''/M''_{max}-\log f$ of the 0.04Nb/0.02Al-CuO ceramics measured at 25, 50 and 75 °C. Each plot of $Z''/Z''_{max}-\log f$ in-

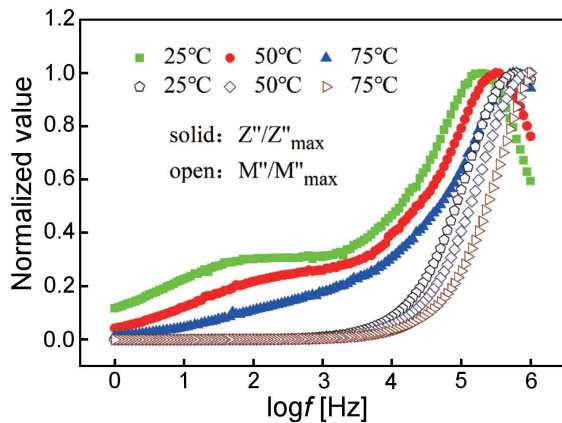


Figure 10. Comparison of the normalized imaginary part of impedance (Z''/Z''_{max}) and electrical modulus (M''/M''_{max}) of 0.04Nb/0.02Al-CuO ceramics at 25, 50 and 75 °C

cludes a broad peak at higher frequency and a weak peak at lower frequency, which represent the grain effect and grain boundary effect, respectively. It can be seen that Z''/Z''_{max} and M''/M''_{max} peaks are in mismatch at each temperature, indicating the presence of localized conduction such as polaron hopping conduction in the NACO ceramics. This is in agreement with the ones discussed in Fig. 9.

As discussed above, the band conduction model and polaron hopping conduction model together contribute to the NTC character of NACO ceramics. The band conduction is caused by the long-range transport of electrons or holes, which usually occurs in the grain interior. In NACO ceramics, electrons occur from the dopant ions, e.g. Al^{3+} doping (Eq. 4) and Nb_2O_5 doping (Eq. 5). Those weakly bound electrons produced by the above electron defect chemistry reactions can be easily activated and jump to the conduction level, resulting in the electronic conduction as so-called band conduction. Usually at low temperatures, band conduction contributes more to the conductivity of ceramics than hopping conduction. For the hopping conduction, as discussed in Fig. 9b, the polarons hopped between $\text{Cu}^{2+}/\text{Cu}^+$ pairs and $\text{Nb}^{5+}/\text{Nb}^{4+}$ pairs, and they can be expressed as $\text{Cu}^{2+} + \text{Cu}^+ \rightleftharpoons \text{Cu}^+ + \text{Cu}^{2+}$ and $\text{Nb}^{5+} + \text{Nb}^{4+} \rightleftharpoons \text{Nb}^{4+} + \text{Nb}^{5+}$. As the temperature rises, the thermal activation increases and enhances the polaron hopping. During the thermally activated hopping process, the polarons need to get rid of the ionic binding and overcome the lattice barriers, indicating that the conduction model of polaron hopping plays an important role in the NTC characteristics (such as temperature sensitivity B value) in the ceramics.

IV. Conclusions

Al-doped CuO, $x\text{Al-CuO}$ (ACO, $x = 0, 0.005, 0.01, 0.015, 0.02, 0.025, 0.03, 0.04$) and Nb-modified 0.02Al-CuO ceramics (NACO, $y\text{Nb}/0.02\text{Al-CuO}$, $0 \leq y \leq 0.07$) were synthesized using sol-gel method and sintered at 980–1000 °C for 30 min in air. The prepared ceramics have a monoclinic crystalline structure as that of CuO phase and exhibit the typical NTC effect. The NTC materials constant, B value, of the NACO ceramics can be adjusted from 2430 K to 3805 K by changing the Nb-doping concentration. The Hoge-3 equation is the best one for the resistance-temperature calibration for the NACO NTC thermistors among the used Basic equation, Steinhart-Hart equation, Hoge-2 equation and Hoge-3. Both grain effect and grain-boundary effect contribute to the conduction of the NACO ceramics. Two kinds of conduction models, band conduction and polaron hopping conduction, are proposed for the conduction mechanisms in the NACO ceramics.

Acknowledgments: This work is supported by the research funding from the Hunan Wedid Materials Technology Co., Ltd. (No. 738010241) and the National Natural Science Foundation of China (No. 51767021).

§ Supporting material can be downloaded using following link: <https://bit.ly/2vBWaak>

References

- X. Zhang, W. Ren, W. Kong, Q. Zhou, L. Wan, L. Bian, J. Xu, A. Chang, C. Jiang, “Effect of sputtering power on structural, cationic distribution and optical properties of $\text{Mn}_2\text{Zn}_{0.25}\text{Ni}_{0.75}\text{O}_4$ thin films”, *Appl. Surf. Sci.*, **435** (2018) 815–821.
- H. Han, S. Mhin, K.R. Park, K.M. Kim, J. Lee, J.H. Ryu, “Fe doped Ni-Mn-Co-O ceramics with varying Fe content as negative temperature coefficient sensors”, *Ceram. Int.*, **43** (2017) 10528–10532.
- S. Liang, C. Cao, Y. Yuan, H. Li, M. Luo, M. Guo, X. Zhang, “Hydrothermal synthesis of Zn-doped Ni-Mn-Al-O thin films toward high-performance negative temperature coefficient thermistor”, *J. Mater. Sci. Mater. Electron.*, **29** (2018) 9025–9032.
- H.S. Han, K.R. Park, Y.R. Hong, K. Shim, S. Mhin, “Effect of Fe incorporation on cation distributions and hopping conduction in Ni-Mn-Co-O spinel oxides”, *J. Alloys Compd.*, **732** (2018) 486–490.
- D. Li, S. Zhao, K. Xiong, H. Bao, C. Nan, “Aging improvement in Cu-containing NTC ceramics prepared by co precipitation method”, *J. Alloys Compd.*, **582** (2014) 283–288.
- M. Schubert, C. Münch, S. Schuurman, V. Poulain, J. Kita, R. Moos, “Characterization of nickel manganite NTC thermistor films prepared by aerosol deposition at room temperature”, *J. Eur. Ceram. Soc.*, **38** (2018) 613–619.
- A. Basu, A.W. Brinkman, R. Schmidt, “Effect of oxygen partial pressure on the NTCR characteristics of sputtered $\text{Ni}_x\text{Mn}_{3-x}\text{O}_{4+\delta}$ thin films”, *J. Eur. Ceram. Soc.*, **24** (2004) 1247–1250.
- Y. Lei, X. Lin, H. Liao, “Effect of Ni, Fe and Mn in different proportions on microstructure and pollutant-catalyzed properties of Ni-Fe-Mn-O negative temperature coefficient ceramic nanocompositions”, *Mater. Chem. Phys.*, **194** (2017) 128–136.
- Y. Zeng, Z.C. Li, J.M. Shao, X.C. Wang, W.B. Hao, H. Zhang, “Electrical properties of perovskite YFeO_3 based ceramics modified by Cu/Nb ions as negative temperature coefficient thermistors”, *J. Mater. Sci. Mater. Electron.*, **30** (2019) 14528–14537.
- W. Fu, Z. Li, P. Li, Y. Zeng, H. Zhang, “Electrical property and temperature sensitivity of $\text{NiFe}_{2-x}\text{Sb}_x\text{O}_4$ ($x \leq 0.02$) ceramics for negative temperature coefficient thermistors”, *J. Mater. Sci. Mater. Electron.*, **29** (2018) 11637–11645.
- Y. Zhao, C. Zhao, J. Huang, B. Zhao, “ LaMnO_3 - $\text{Ni}_{0.75}\text{Mn}_{2.25}\text{O}_4$ supported bilayer NTC thermistors”, *J. Am. Ceram. Soc.*, **97** (2014) 1016–1019.
- X. Sun, Z. Li, W. Fu, S. Chen, H. Zhang, “Li/Fe modified $\text{Zn}_{0.3}\text{Ni}_{0.7}\text{O}$ NTC thermistors with adjustable resistivities and temperature sensitivity”, *J. Mater. Sci. Mater. Electron.*, **29** (2018) 343–350.
- J. Zhang, H. Zhang, B. Yang, Y. Zhang, Z. Li, “Temperature sensitivity of Fe-substituted SnO_2 -based ceramics as negative temperature coefficient thermistors”, *J. Mater. Sci. Mater. Electron.*, **27** (2016) 4935–4942.
- Z. He, Z. Li, Q. Xiang, W. Yan, H. Zhang, “Electrical properties of Y/Mg modified NiO simple oxides for negative temperature coefficient thermistors”, *Int. J. Appl. Ceram. Tech.*, **16** (2019) 160–169.
- Z. Yang, H. Zhang, Z. He, B. Li, Z. Li, “Influence of B^{3+} - and Na^+ -ions on electrical property and temperature sensitivity of NiO-based ceramics”, *J. Mater. Sci. Mater. Electron.*, **3** (2019) 3088–3097.
- X. Sun, S. Leng, H. Zhang, Z. He, Z. Li, “Electrical properties and temperature sensitivity of Li/Mg modified $\text{Ni}_{0.7}\text{Zn}_{0.3}\text{O}$ based ceramics”, *J. Alloys Compd.*, **763** (2018) 975–982.
- Z. Guo, J. Shao, H. Lin, M. Jiang, S. Chen, Z. Li, “Electrical conductivity & temperature sensitivity of ceramics based on NiO simple oxides for NTC applications”, *J. Mater. Sci. Mater. Electron.*, **28** (2017) 11871–11877.
- S.Y. Wang, S.F. Yu, M. Lu, M.Z. Liu, L. Zuo, “Atomic layer-deposited titaniumdoped vanadium oxide thin films and their thermistor applications”, *J. Electron. Mater.*, **46** (2017) 2153–2157.
- B. Yang, D. Chen, “Synthesis of CuO nanoparticles for catalytic application via ultrasound-assisted ball milling”, *Process. Appl. Ceram.*, **11** (2017) 39–44.
- J. Zhang, J. Wang, Y. Fu, B. Zhang, Z. Xie, “Sonochemistry-synthesized CuO nanoparticles as an anode interfacial material for efficient and stable polymer solar cells”, *RSC Adv.*, **5** (2015) 28786–28793.
- W. Chen, H. Zhang, Z. Ma, S. Li, Z. Li, “Binder free $\text{Cu}(\text{OH})_2/\text{CuO}$ electrodes fabricated directly on copper foils by facile large-scale production method”, *J. Alloys Compd.*, **762** (2018) 565–573.
- J. Lu, W. Xu, S. Li, W. Liu, M.S. Javed, G. Liu, C. Hu, “Rational design of CuO nanostructures grown on carbon fiber fabrics with enhanced electrochemical performance for flexible supercapacitor”, *J. Mater. Sci.*, **53** (2018) 739–748.
- W. Chen, H. Zhang, B. Yang, B. Li, Z. Li, “Characterization of $\text{Cu}_3\text{N}/\text{CuO}$ thin films derived from annealed Cu_3N for electrode application in Li-ion batteries”, *Thin Solid Films*, **672** (2019) 157–164.
- Y.H. Elbasha, A.M. Badr, H.A. Elshaikh, A.G. Mostafa, A.M. Ibrahim, “Dielectric and optical properties of CuO containing sodium zinc phosphate glasses”, *Process. Appl. Ceram.*, **10** (2016) 277–286.
- B. Yang, H. Zhang, J. Guo, Y. Liu, Z. Li, “Electrical properties and thermal sensitivity of Ti/Y modified CuO-based ceramic thermistors”, *Front. Mater. Sci.*, **10** (2016) 413–421.
- G. Liu, L. Guo, C. Liu, Q. Wu, “Evaluation of different calibration equations for NTC thermistor applied to high-precision temperature measurement”, *Measurement*, **120** (2018) 21–27.
- F. Du, Q. Chen, Y. Wang, “Effect of annealing process on the heterostructure $\text{CuO}/\text{Cu}_2\text{O}$ as a highly efficient photocathode for photoelectrochemical water reduction”, *J. Phys. Chem. Solids.*, **104** (2017) 139–144.
- X. Ma, Y. Chen, J. Lee, C. Yang, X. Cui, “In situ formation of NbO_x/NbN microcomposites: seeking potential in photocatalytic and Li-ion battery applications”, *New. J. Chem.*, **42** (2018) 1300–1308.
- A. Feteiraw, “Negative temperature coefficient resistance (NTCR) ceramic thermistors: an industrial perspective”, *J. Am. Ceram. Soc.*, **92** (2009) 967–983.
- S. Rudtsch, C.V. Rohden, “Calibration and self-validation of thermistors for high-precision temperature measurements”, *Measurement*, **76** (2015) 1–6.
- M.A. Rafiq, M.T. Khan, Q.K. Muhammad, M. Waqar,

- F. Ahmed, “Impedance analysis and conduction mechanism of Ba doped $\text{Mn}_{1.75}\text{Ni}_{0.7}\text{Co}_{0.5-x}\text{Cu}_{0.05}\text{O}_4$ NTC thermistors”, *Appl. Phys. A*, **123** (2017) 589–597.
32. P.K. Panda, D. Behera, “Investigation of electric transport behavior of bulk CoFe_2O_4 by complex impedance spectroscopy”, *J. Alloys. Compd.*, **587** (2014) 481–486.
33. R. Gerhardt, “Impedance and dielectric spectroscopy revisited: Distinguishing localized relaxation from long-range conductivity”, *J. Phys. Chem. Solids.*, **55** (1994) 1491–1506.